Journal of Controlled Release 209 (2015) 327–336

Contents lists available at ScienceDirect

Journal of Controlled Release

journal homepage: www.elsevier.com/locate/jconrel

Enhanced delivery of liposomes to lung tumor through targeting interleukin-4 receptor on both tumor cells and tumor endothelial cells

Lianhua Chi [a,b,c,1], Moon-Hee Na [a,1], Hyun-Kyung Jung [a,c], Sri Murugan Poongkavithai Vadevoo [a,b,c], Cheong-Wun Kim [a,b,c], Guruprasath Padmanaban [a,c], Tae-In Park [d], Jae-Yong Park [e], Ilseon Hwang [f], Keon Uk Park [f], Frank Liang [g], Maggie Lu [g], Jiho Park [h], In-San Kim [i], Byung-Heon Lee [a,b,c,*]

[a] Department of Biochemistry and Cell Biology, Kyungpook National University, Daegu, Republic of Korea
[b] BK21 Plus KNU Biomedical Convergence Program, Department of Biomedical Science, Kyungpook National University, Daegu, Republic of Korea
[c] CMRI, Kyungpook National University, Daegu, Republic of Korea
[d] Department of Pathology, Kyungpook National University, Daegu, Republic of Korea
[e] Department of Internal Medicine, School of Medicine, Kyungpook National University, Daegu, Republic of Korea
[f] Dongsan Medical Center, Daegu, Republic of Korea
[g] Industrial Technology Research Institute, HsinChu, Taiwan
[h] Department of Bio and Brain engineering, KAIST, Daejeon, Republic of Korea
[i] Biomedical Center, Korea Institute of Science and Technology, Seoul, Republic of Korea

ARTICLE INFO

Article history:
Received 20 January 2015
Received in revised form 7 May 2015
Accepted 9 May 2015
Available online 12 May 2015

Keywords:
IL-4 receptor
Liposomes
Lung tumor
Targeted drug delivery

ABSTRACT

A growing body of evidence suggests that pathological lesions express tissue-specific molecular targets or biomarkers within the tissue. Interleukin-4 receptor (IL-4R) is overexpressed in many types of cancer cells, including lung cancer. Here we investigated the properties of IL-4R-binding peptide-1 (IL4RPep-1), a CRKRLDRNC peptide, and its ability to target the delivery of liposomes to lung tumor. IL4RPep-1 preferentially bound to H226 lung tumor cells which express higher levers of IL-4R compared to H460 lung tumor cells which express less IL-4R. Mutational analysis revealed that C1, R2, and R4 residues of IL4RPep-1 were the key binding determinants. IL4RPep-1-labeled liposomes containing doxorubicin were more efficiently internalized in H226 cells and effectively delivered doxorubicin into the cells compared to unlabeled liposomes. *In vivo* fluorescence imaging of nude mice subcutaneously xenotransplanted with H226 tumor cells indicated that IL4RPep-1-labeled liposomes accumulate more efficiently in the tumor and inhibit tumor growth more effectively compared to unlabeled liposomes. Interestingly, expression of IL-4R was high in vascular endothelial cells of tumor, while little was detected in vascular endothelial cells of control organs including the liver. IL-4R expression in cultured human vascular endothelial cells was also up-regulated when activated by a pro-inflammatory cytokine tumor necrosis factor-α. Moreover, the up-regulation of IL-4R expression was observed in primary human lung cancer tissues. These results indicate that IL-4R-targeting nanocarriers may be a useful strategy to enhance drug delivery through the recognition of IL-4R in both tumor cells and tumor endothelial cells.

1. Introduction

Lung cancer is one of the leading causes of cancer death worldwide. Few biomarkers of lung cancer cells have been known as a target for molecular therapy. One promising target for non-small cell lung cancer (NSCLC) is the epidermal growth factor receptor (EGFR) with activating mutations, such as the L858R mutation. Targeted therapy with EGFR kinase inhibitors, such as erlotinib and gefitinib, extends progression-free survival (PFS) of patients with activating EGFR mutation-positive NSCLC [1,2]. However, the activating mutation of EGFR is only present in a portion of patients (approximately 20%) with NSCLC. In addition, although the median PFS of the erlotinib-treated patients was longer than that of chemotherapy-treated patients, it was still limited to approximately one year [1,2]. This limited PFS may be caused by the onset of adaptive resistance to the targeted therapies. For example, inhibition of EGFR with erlotinib can inhibit its downstream signaling pathways but eventually leads to compensatory up-regulation of other signaling pathways including mesenchymal–epithelial transition factor (MET) amplification or target modification such as the EGFR T790M mutation [3,4]. Combination of targeted therapeutics may help overcome the adaptive resistance and prolong PFS but will inevitably increase the cost for treatment. Furthermore, intertumoral and intratumoral heterogeneity

* Corresponding author at: Department of Biochemistry and Cell Biology, School of Medicine, Kyungpook National University, 680 Gukchaebosangro, Junggu, Daegu 700-842, Republic of Korea.
E-mail address: leebh@knu.ac.kr (B.-H. Lee).
[1] These authors equally contributed.

http://dx.doi.org/10.1016/j.jconrel.2015.05.260
0168-3659/

of human cancer [5] may complicate the combination of targeted therapies.

Conventional chemotherapeutic agents, such as doxorubicin acting on DNA replication and paclitaxel acting on microtubule assembly during cell proliferation, have been effective anti-cancer agents. As systemic side effects due to toxicity to normal tissues have limited the usage of chemotherapeutic agents, targeted delivery of these agents to the tumor tissue will possibly reduce their systemic side effects and enhance the efficacy of the therapeutics. In addition, unlike targeted therapies using antibodies or receptor tyrosine kinase inhibitors, conventional chemotherapeutic drugs may have less risk of inducing compensatory signaling pathways and subsequent adaptive resistance to the therapy. Moreover, targeted delivery of chemotherapeutic agents would be more affordable than targeted therapies using expensive antibodies.

Interleukin-4 receptor (IL-4R) is up-regulated in many types of tumor cells including lung cancer, head and neck cancer, and glioblastoma [6–8]. In solid tumors, IL-4R is a heterodimer composed of IL-4Rα and IL-13Rα1 and binds with interleukin-4 (IL-4) or interleukin-13 (IL-13) [9]. IL-4 protein fused with *Pseudomonas* exotoxin has been exploited as a targeted cytotoxin to IL-4R-overexpressing tumors [6,10,11]. Using phage-displayed random peptides, we previously identified a peptide that binds to IL-4R, named IL-4R-binding peptide-1 (IL4RPep-1), with the sequence of CRKRLDRNC [12]. This sequence is homologous to the ^{84}KRLDRN^{89} motif in the IL-4R-binding domain of human IL-4. Although peptides usually have weaker binding affinity and stability than antibodies, they generally have more efficient tissue penetration ability due to smaller size, and multimeric labeling of peptides onto nanocarriers may improve their binding avidity and stability [13–15]. In support of this, IL4RPep-1 has been exploited as a targeting ligand on drug-loaded nanocarriers and successfully enhanced drug delivery to tumors [16–19]. Here we characterized the binding activity, stability, and localization of IL4RPep-1 in tumor tissue, and report that it enhances the delivery of liposomes to lung tumor by targeting IL-4R, which is up-regulated in both tumor cells and tumor endothelial cells.

2. Materials and methods

2.1. Cell culture

H226 human squamous NSCLC and H460 human large cell NSCLC cell lines were cultured with RPMI-1640 medium supplemented with 10% fetal bovine serum and penicillin/streptomycin. Human umbilical vein endothelial cells (HUVECs) were cultured with EGM-2 medium.

2.2. Synthesis of peptides

Wild-type IL4RPep-1 (CRKRLDRNC) or mutant peptides were synthesized by Peptron Inc. (Daejeon, Korea). Fluorescein isothiocyanate (FITC) or biotin was conjugated to the N-terminal of each peptide during peptide synthesis. Lyophilized peptides were reconstituted with dimethyl sulfoxide (DMSO) to a concentration of 100 mM and then diluted with phosphate-buffered saline (PBS) to a concentration of 10 μM. Mutant IL4RPep-1 peptides include those with the substitution of cysteine at N-terminal to alanine (C1A, ARKRLDRNC), arginine at the second residue to alanine (R2A, CAKRLDRNC), lysine at the third residue to alanine (K3A, CRARLDRNC), arginine at the fourth residue to alanine (R4A, CRKALDRNC), leucine at the fifth residue to alanine (L5A, CRKRADRNC), aspartic acid at the sixth residue to alanine (D6A, CRKRLARNC), arginine at the seventh residue to alanine (R7A, CRKRLDANC), asparagine at the eighth residue to alanine (N8A, CRKRLDRAC), and cysteine at C-terminal to alanine (C9A, CRKRLDRNA). NSSSVDK, a peptide sequence present in the phage coat protein, was used as a control peptide.

2.3. Cellular binding and internalization of peptides and liposomes

H226 or H460 cells (1×10^5 cells per well) were seeded onto eight-well chamber slides. After overnight culture, cells were incubated with PBS containing 1% bovine serum albumin (BSA) at 37 °C for 30 min for reducing non-specific binding of peptides to plastic plates. For peptide binding assays, cells were incubated with a 10 μM solution of FITC-conjugated IL4RPep-1 or each mutant peptide in 200 μl PBS per well at 4 °C for 1 h. For liposome binding assays, cells were incubated with Cy5.5 fluorescence dyes-labeled liposomes (1:30 diluted with PBS) containing IL4RPep-1 at a concentration of 10 μM at 4 °C for 1 h. For internalization assays, cells were incubated with peptides or liposomes at 37 °C for 1 h. After incubation with the peptides or liposomes, cells were washed with PBS three times for three minutes each time. After washing, cells were fixed with 4% paraformaldehyde (PFA) and mounted with an anti-fade reagent (Life Technologies, Carlsbad, CA). Nucleus was counterstained with a 200 μl solution of 4′,6′-diamidino-2-phenylindole (DAPI, Sigma-Aldrich, St Louis, MO). Cells were observed with a confocal microscope (Zeiss, Oberkochen, Germany) with the excitation/emission wavelengths of 488 nm/520 nm and 633 nm/690 nm for FITC and Cy5.5, respectively.

To examine the binding of IL4RPep-1 to cytokine-activated HUVECs, cells were incubated with 1 ng/ml of tumor necrosis factor-α (TNF-α) in 200 μl PBS per well for 24 h. After treatment, cells were incubated with a 10 μM solution of IL4RPep-1 at 4 °C for 1 h. Cells were also stained with an anti-human IL-4Rα antibody (1:200 dilution, R&D systems, Minneapolis, MN) at RT for 1.5 h and then with Alexa Fluor 594-conjugated secondary antibodies. After fixation and mounting, cells were counterstained with DAPI and observed under a fluorescence microscope (Olympus, Tokyo, Japan) with excitation/emission wavelengths of 490 nm/520 nm and 590 nm/617 nm for FITC and Alexa Fluor 594, respectively.

For flow cytometry, cells (1×10^6 cells) were harvested and suspended in culture medium containing 1% BSA at 37 °C for 30 min for blocking and then incubated with a 10 μM solution of wild-type or mutant IL4RPep-1 peptides in serum-free medium at 4 °C for 1 h. After washing, a 300 μl of cell suspension in PBS was subjected to flow cytometry (BD, Franklin Lakes, NJ) with excitation/emission wavelengths of 488 nm/530 nm for FITC.

2.4. Saturation binding assays

H226 or H460 cells in a 96-well plate (5×10^4 cells per well) were blocked with 1% BSA for 30 min at room temperature (RT) and incubated with biotin-labeled IL4RPep-1 (1 to 80 μM) at 4 °C for 1 h. After washing, cells were incubated with NeutrAvidin-horse radish peroxidase (HRP) (1:10000 dilution) for 30 min at RT. HRP activity was measured using 3,3′,5,5′-tetramethylbenzidine as a substrate (Thermo Fisher Scientific, Waltham, MA), and the reaction was halted using 2 M sulfuric acid. Absorbance was measured at 450 nm using a microplate reader. The binding affinity (Kd value) was calculated using GraphPad Prism 6 (GraphPad Software Inc., La Jolla, LA).

2.5. Serum stability of IL4RPep-1

Mouse blood was collected and allowed to clot. Serum was obtained by centrifugation of blood clots at 4 °C twice followed by filtration through 0.22 μm pore. IL4RPep-1 (100 μg in 50 μl of PBS) was incubated with 50 μl of filtered serum at 37 °C for the indicated time periods. The incubated samples were diluted 100-fold and fractionated by C18 reverse phase high performance liquid chromatography (HPLC) with a linear gradient of acetonitrile (Vydac protein and peptide C18, 0.1% trifluoroacetate in water for equilibration, and 0.1% trifluoroacetate in acetonitrile for elution). The peptide peak was collected and vacuum dried, and the molecular weight of the peptide was confirmed by MALDI-TOF mass spectrometer (Life Technologies).

2.6. Preparation of IL4RPep-1-labeled liposomes containing doxorubicin

Cholesterols, hydrogenated soybean L-α-phosphatidylcholine (HSPC), 1,2-diacyl-sn-glycero-3-phosphoethanolamine-N-[methoxy (polyethylene glycol)-2000] (DSPE-PEG_{2000}), and 1,2-distearoyl-sn-glycero-3-phosphoethanolamine-N-[maleimide(polyethyleneglycol)-2000] (DSPE-PEG_{2000}-MAL) were purchased from Avanti Polar Lipids. Briefly, all lipids (HSPC: cholesterol: DSPE-PEG2000 = 6:4:0.5 by molar ratio) for the preparation of liposomes were dissolved in 60 °C ethanol and then injected into a water phase (1:10 by volume) at 60 °C for 1 h for hydration. Following hydration, liposomes were extruded 6 times through polycarbonate filters (0.2 μm pore size), followed by extrusion 6 times through additional filters (0.05 μm pore size). Particle size of prepared liposomes was determined by dynamic light scattering (typically 80–120 nm). For encapsulation of doxorubicin, a standard remote-loading method using ammonium sulfate was employed. The water phase in the liposome preparation was 250 mM $(NH_4)_2SO_4$. After extruding liposomes, the placebo liposomes were put into a dialysis membrane against large quantity of 10% sucrose containing 5 mM NaCl to remove the outer ammonium sulfate of liposomes. Subsequently, doxorubicin HCl was added to the liposomal dispersion to achieve a dose of 2 mg doxorubicin/ml. The loading process was carried out at 60 °C for 1 h and then quickly cooled down. For the incorporation of Cy5.5 amidite into liposomes, these dyes were mixed with all lipids in ethanol to be injected into the PBS solution. Due to the hydrophobic property of these dyes, they were trapped in the bilayer region of liposomes. For IL4RPep-1 labeling of liposomes, the post-insertion method was used. IL4RPep-1 was previous conjugated to DSPE-PEG_{2000}-MAL by a molar ratio of 1:2 and then was post-inserted into plain liposomes at 60 °C for 1 h. The amount of IL4RPep-1 was set to 1.5% molar ratio of total lipids.

2.7. In vivo fluorescence imaging and anti-tumor therapy

All animal experiments were conducted according to the guidelines of Kyungpook National University Ethical Committee. H226 tumor cells (5×10^6 cells) were subcutaneously injected into the right flank of 6 week-old BALB/c nude mice. A 100 μl solution of IL4RPep-1-labeled and unlabeled liposomes containing Cy5.5 was intravenously injected into tumor-bearing mice and circulated for 2 h. *In vivo* imaging was conducted by scanning mice under anesthesia using Optix exPlore (ART, Montreal, Canada). After imaging, tumor and organs were isolated for immunhistochemistry.

For anti-tumor therapy, treatments were started after 2–3 weeks from the day of tumor cell injection, when tumor volumes reached approximately 50 mm^3. Tumor-bearing mice were intravenously injected with liposomes containing doxorubicin (at a dose of 1 mg/kg body weight, two times per week for a total of seven injections). Tumor volumes were calculated using the following equation: length × $(width)^2$ × 0.52.

2.8. Immunofluorescence of IL-4R expression of cultured cells and tissues

H226 or H460 cells (1×10^5 cells per well) were seeded onto eight-well chamber slides and cultured overnight. Cells were fixed for 3 min with methanol:acetone (2:1) and blocked with 1% BSA/5% normal goat serum in PBS. Cells were incubated with anti-human IL-4Rα (1:200 dilution) for 1 h at RT and then incubated with FITC- or Alexa Fluor 594-conjugated secondary antibody (1:200 dilution) for 30 min at RT. After DAPI counterstaining and mounting, cells were observed under a fluorescence microscope. For tissue staining, tumor and organs were isolated after perfusion of a mouse with PBS and subsequently with 4% paraformaldehyde (PFA). Isolated tissues were fixed in 4% PFA, sequentially subjected to 10%, 20%, and 30% sucrose solution overnight, and then embedded in the OCT™ compound (Sakura, Alphen aan den Rijn, Netherlands). Frozen tissues were sectioned at 7 μm thickness. After incubation in a blocking solution (1% BSA/5% normal goat serum in PBS), tissues were incubated with anti-human IL-4Rα (1:200 dilution), anti-mouse IL-4Rα (1:200 dilution, BD), or anti-mouse CD31 (1:100 dilution, BD) antibodies at RT for 1.5 h and then incubated with secondary antibodies. Sections were mounted, counterstained with DAPI, and observed under a fluorescence microscope.

2.9. IL-4R staining of primary lung cancer tissues

Paraffin-embedded biopsy specimens of lung cancer were obtained, and tissue microarrays were constructed from the tissue blocks. After tissue preparation for immunohistochemistry, tissue sections were incubated with anti-human IL-4Rα antibody (1:200 dilution) at 4 °C overnight and then incubated with secondary antibody. After antibody staining, tissues were counterstained with hematoxylin. Samples were analyzed by an experienced pathologist, and the staining intensity was scored as strong or weak.

2.10. Statistical analysis

Statistical analysis was performed by one-way ANOVA test with Bonferroni post-test.

3. Results

3.1. Binding of IL4RPep-1 to IL-4R-expressing tumor cells and its serum stability

To examine the binding of IL4RPep-1 to lung tumor cells, two human lung tumor cell lines, H226 and H460, were used. Immunofluorescence staining with anti-human IL-4Rα antibody showed that H226 cells express IL-4R at much higher levels than H460 cells (Fig. 1A). Subsequently, the binding of IL4RPep-1 to H226 cells was high, while little binding to H460 cells was observed (Fig. 1A). In addition, IL4RPep-1 was efficiently internalized into H226 cells within 2 h, as shown in a Z-section obtained by a confocal microscopy (Fig. 1A). When analyzed by saturation binding assays, the binding affinity (Kd) of IL4RPep-1 to H226 cells was much higher than that to H460 cells (6.5 μM *versus* 51.9 μM, Fig. 1B), which was in the same context with the difference in the levels of IL-4R expression on those cells.

To determine which amino acid residues are important for the binding of IL4RPep-1, each amino acid residue was mutated to alanine. C1A, R2A, and R4A mutations remarkably reduced the binding of each peptide to H226 cells to approximately 20% of wild-type IL4RPep-1 ($p < 0.001$, Fig. 1C). L5A and N8A mutations reduced the cell binding of each peptide to approximately 40% and 60% of wild-type peptide, respectively ($p < 0.01$, Fig. 1C). On the other hand, K3A, D6A, R7A, and C9A mutations did not significantly decrease the cell binding of each peptide (Fig. 1C). In addition, a cyclic form of IL4RPep-1 containing a disulfide bonding between C1 and C9 showed slightly weaker cell binding activity compared to the wild-type IL4RPep-1 which was in a linear form (data not shown). We used the linear form of wild-type IL4RPep-1 for further studies.

To examine the stability of IL4RPep-1, it was incubated with whole serum obtained from mice up to 24 h. The peptide peak was not decreased until 4 h after incubation with serum and, while slowly declined thereafter, most of it was still maintained at 24 h after incubation (Fig. 2). These results demonstrate that IL4RPep-1 was not degraded and stable at least up to 4 h in the presence of serum.

3.2. Cell binding and intracellular uptake of IL-4R-targeting liposomes

As an IL-4R-targeting nanocarrier, IL4RPep-1-labeled or unlabeled liposomes containing doxorubicin (IL4RPep-1-L-Dox and L-Dox, respectively) were prepared. Both liposomes were labeled with Cy5.5 fluorescence dye. The average size of L-Dox and IL4RPep-1-L-Dox

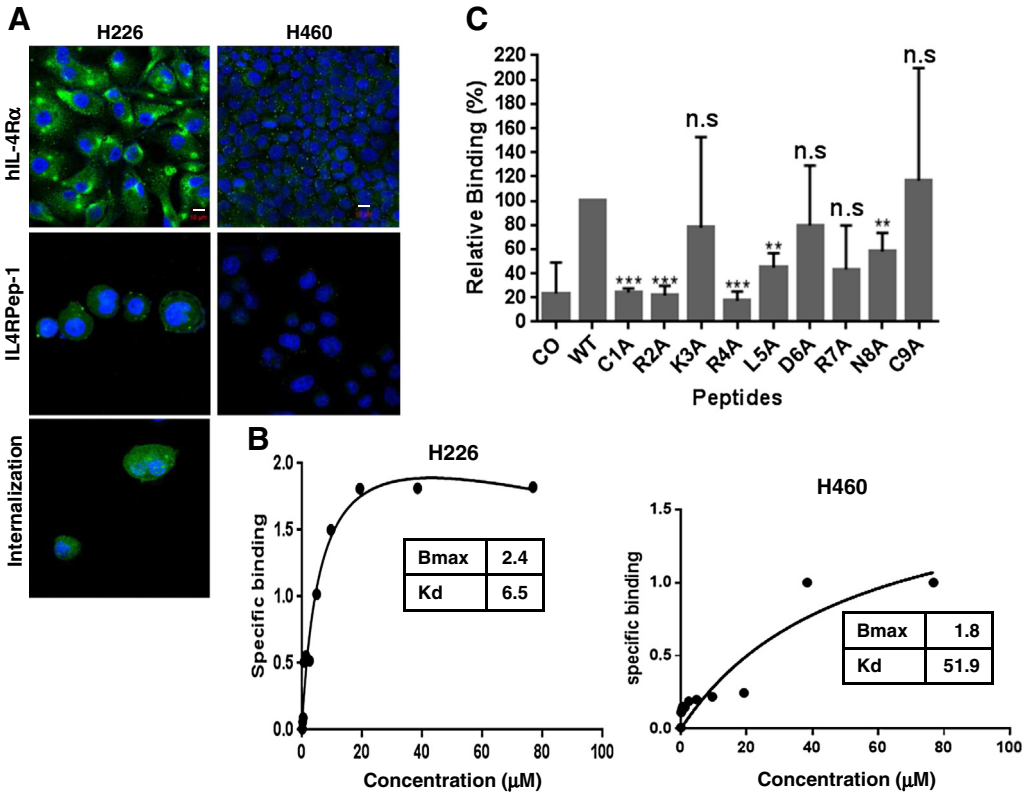

Fig. 1. Expression of IL-4R on human lung tumor cell lines and the cell binding of IL4RPep-1. (A) H226 and H460 cells were stained with anti-human IL-4Rα antibody (upper panel, green) or incubated with FITC-labeled IL4RPep-1 (middle panel, green). A confocal Z-section image of H226 cells after incubation with FITC-labeled IL4RPep-1 for 2 h was taken (lower panel, green). Nuclei were counter-stained with DAPI dye. Scale bars, 10 μm. (B) Saturation binding assays. H226 and H460 cells were incubated with biotin-labeled IL4RPep-1. The cell-bound peptide was detected by NeutrAvidin-HRP and subsequent color reaction using a substrate. (C) Mutational analysis. H226 cells were incubated with FITC-labeled wild-type IL4RPep-1 and its mutants. Percent cell binding of each peptide was measured by flow cytometry and was represented as relative binding to that of wild type. CO, control; WT, wild-type. (For interpretation of the references to color in this figure legend, the reader is referred to the web version of this article.)

were 97 nm and 100 nm, respectively (Fig. 3A). The average zeta potential of L-Dox and IL4RPep-1-L-Dox were −23.2 mV and −32.6 mV, respectively (Fig. 3B). IL4RPep-1-L-Dox bound to H226 cells at higher levels than to H460 cells, while the binding of unlabeled L-Dox to both cell lines was low (Fig. 4A). Higher levels of intracellular uptake of liposomes were detected in H226 cells after incubation with IL4RPep-1-L-Dox than with L-Dox, while those levels were low in H460 cells after incubation with either IL4RPep-1-L-Dox or L-Dox (Fig. 4B). Subsequently, higher levels of doxorubicin were observed in the nucleus of H226 cells after incubation with IL4RPep-1-L-Dox than with L-Dox, as examined by the autofluorescence of doxorubicin (Fig. 4C). These results showed that IL4RPep-1, as a targeting moiety, enabled liposomes to preferentially bind to IL-4R-expressing cells and more efficiently deliver doxorubicin into the cells.

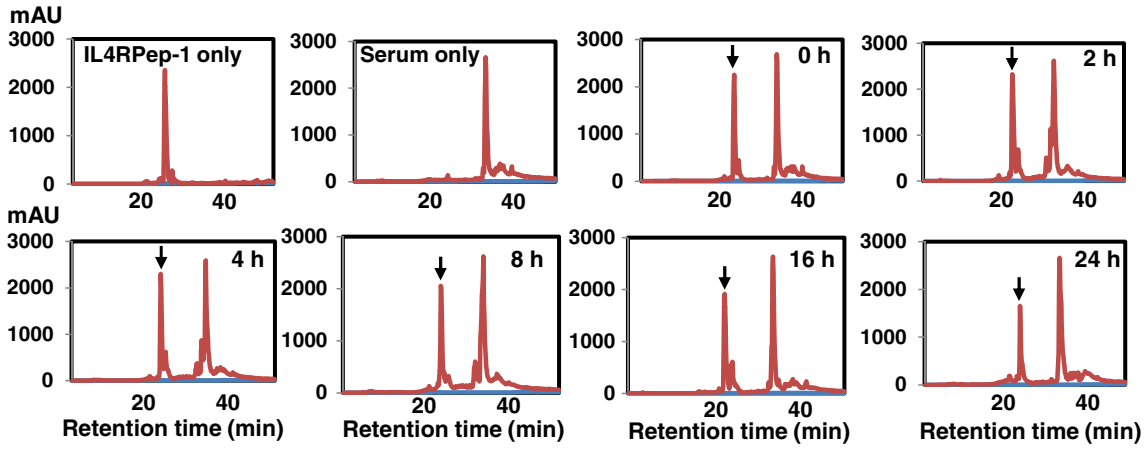

Fig. 2. The serum stability of IL4RPep-1. IL4RPep-1 was incubated with mouse serum at 37 °C for the indicated time periods (0–24 h). Samples were fractionated by C18 reverse-phase HPLC. Samples containing peptide or serum only were used as controls. Y axis represents milli absorbance unit (mAU) at 215 nm. X axis represents the retention time in minutes. The peptide peak was indicated by an arrow and separable from serum peaks.

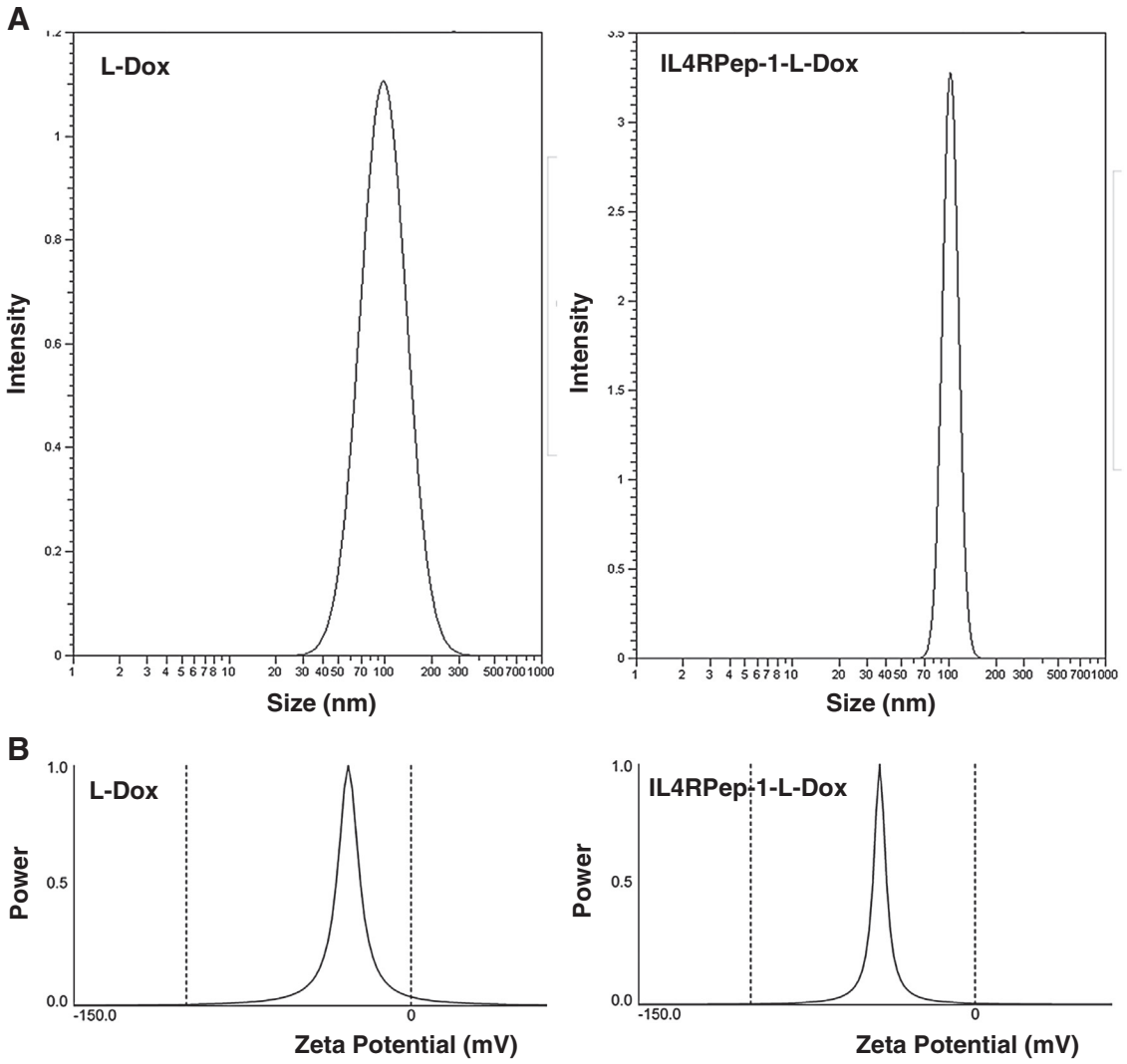

Fig. 3. The sizes and zeta potentials of liposomes. IL4RPep-1-labeled (IL4RPep-1-L-Dox) or unlabeled (L-Dox) liposomes containing doxorubicin were prepared, and their sizes (A) and zeta potentials (B) were measured.

3.3. In vivo tumor homing of IL-4R-targeting liposomes and anti-tumor growth activity

In order to examine tumor homing of IL-4R-targeting liposomes, IL4RPep-1-labeled liposomes were systemically administered into H226 tumor-bearing mice and followed by *in vivo* fluorescence imaging. IL4RPep-1-labeled liposomes were accumulated at tumor site at higher levels than unlabeled liposomes with the maximum fluorescence signals at 1 h after injection of liposomes (Fig. 5A). When tumor and control organs were isolated at 4 h after injection and observed *ex vivo*, little fluorescence intensities by the accumulation of liposomes at control organs such as lung, spleen, and heart were observed, whereas fluorescence intensities by the accumulation of liposomes, regardless of IL-4R-targeting, at the liver were higher than those at tumor (data not shown).

Antitumor growth activity of doxorubicin-loaded liposomes was examined on mice bearing a H226 tumor xenograft. The dose of doxorubicin given for this study was at 1 mg/kg body weight. At this dose, doxorubicin alone showed only mild antitumor growth activity (Fig. 5B). On the other hand, IL-4R-targeting liposomes containing an equivalent dose of doxorubicin significantly inhibited tumor growth compared to untreated control and doxorubicin alone ($p < 0.001$) and untargeted liposomes ($p < 0.05$) (Fig. 5B). Body weights of animals were similar among experimental groups during the treatment (Fig. 5C).

3.4. Localization of IL-4R-targeting liposomes and IL-4R at tumor tissues

Immunofluorescence analysis of tumor tissues showed that IL-4R-targeting liposomes were accumulated at H226 tumor xenografts at higher levels than untargeted liposomes (Fig. 6A). Interestingly, IL-4R-targeting liposomes were particularly accumulated at perivascular tumor cells and blood vessels (Fig. 6A). This led us to hypothesize that IL-4R is up-regulated not only on tumor cells but also on the endothelial cells of blood vessels. This possibility was examined by staining tumor tissues using anti-mouse IL-4Rα antibody, since tumor blood vessels are mouse origin. It was found that IL-4R was highly expressed in vascular endothelial cells of tumor tissues, (Fig. 6B). In contrast, little or low levels of IL-4R were expressed in vascular endothelial cells of control organs, such as the liver, lung, and spleen of tumor-bearing mice, while there were abundant blood vessels within these tissues (Fig. 6B). Moreover, strong expression of IL-4R in tumor endothelial cells was found in autochthonous lung tumor tissues of the K-ras^{LA2} transgenic mouse (Fig. 6C). This mouse lung cancer model has been known closely similar to human lung cancer [20].

In order to further examine the expression of IL-4R in tumor endothelial cells, cultured HUVECs were treated with a pro-inflammatory cytokine TNF-α, which was based on the hypothesis that such cytokine-activated endothelial cells presumably mimic endothelial cells of blood vessels within tumor microenvironment. The expression of IL-

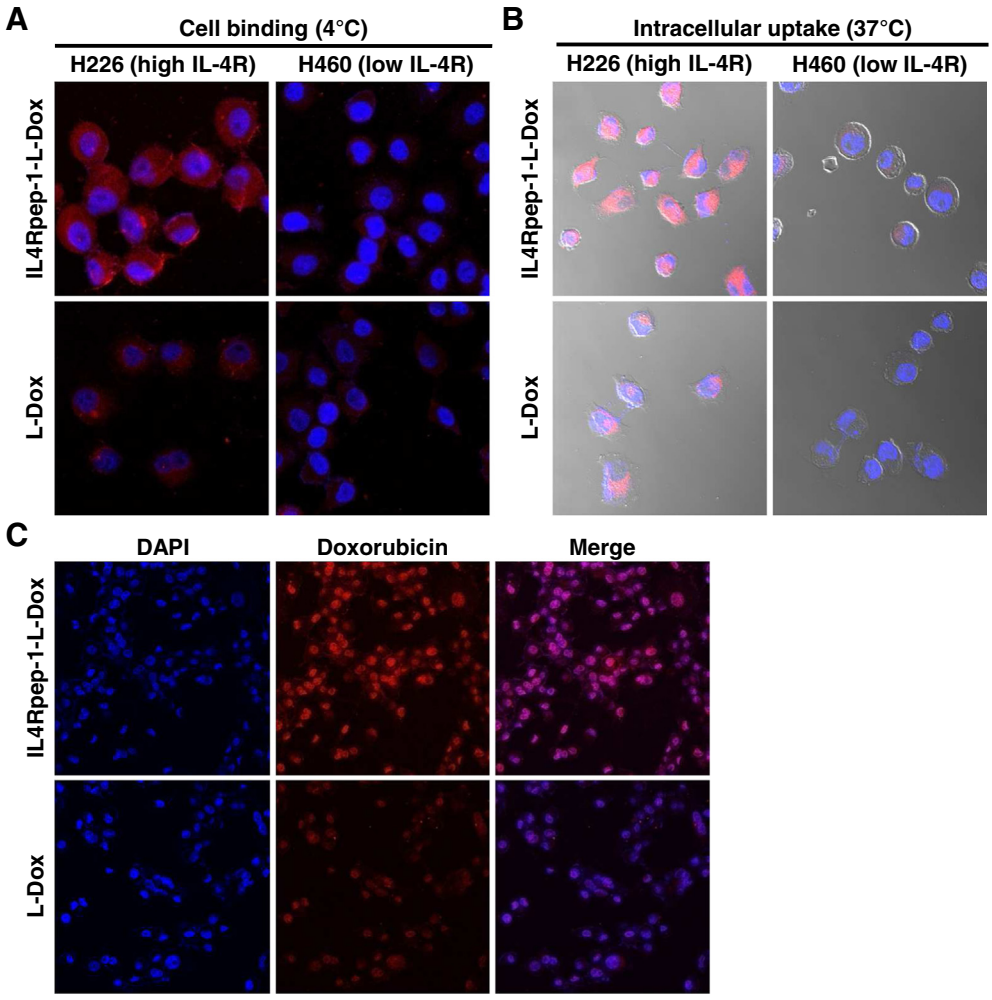

Fig. 4. Cell binding and intracellular uptake of IL-4R-targeting liposomes and doxorubicin delivery to lung tumor cells. (A) Cell binding. H226 and H460 lung tumor cells were incubated with IL4RPep-1-labeled L-Dox or L-Dox at 4 °C for 1 h. Cell binding of liposomes was determined by Cy5.5 fluorescence intensity. (B) Internalization. Cells were incubated with IL4RPep-1-L-Dox or L-Dox at 37 °C for 2 h. Intracellular uptake of liposomes into cells was examined by the merge of light microscopic images and Cy5.5 fluorescence images. (C) Nuclear accumulation of doxorubicin in H226 cells after incubation with IL4RPep-1-L-Dox or L-Dox. Note the co-localization of the autofluorescence of doxorubicin with DAPI nuclear staining.

4R was remarkably increased in TNF-α-activated HUVECs compared to the basal levels of IL-4R expression in untreated cells, and this was accompanied by the increase of IL4RPep-1 binding to the TNF-α-activated cells (Fig. 7).

3.5. Up-regulation of IL-4R in human primary lung tumor tissues

The expression of IL-4R in human primary lung cancer tissues was examined using tissues from 98 cases of squamous cell carcinoma, 65 cases of adenocarcinoma, and 9 cases of large cell carcinoma of NSCLC. Strong staining intensity of IL-4R was observed in 60% of squamous cell carcinoma tissues and 66% of adenocarcinoma tissues, while being observed in 22% of large cell carcinoma tissues (Table 1). Representative microscopic images on IL-4R over-expression in squamous cell carcinoma (Fig. 8B) and adenocarcinoma tissues (Fig. 8D) were shown. Of interest, IL-4R expression was also up-regulated in peritumoral blood vessels of squamous cell carcinoma (Fig. 8C) and tumor-surrounding stroma regions of adenocarcinoma (Fig. 8E).

4. Discussion

This study shows that IL-4R-targeting liposomes which are labeled with IL4RPep-1 as a ligand preferentially deliver drugs to tumor by recognizing IL-4R not only on tumor cells but also on tumor endothelial cells and exert more efficient anti-tumor growth activity compared to untargeted liposomes in a human lung tumor xenograft model on mouse. In addition, the IL4RPep-1 peptide was efficiently internalized into IL-4R-expressing cells on culture and enhanced the cellular uptake of doxorubicin-loaded liposomes. It is expected that the binding of IL-4R targeted liposomes to IL-4R on tumor vascular endothelium enables the nanocarriers to recognize tumor blood vessels during circulation, where many of them would extravasate in collaboration with the enhanced permeability and retention (EPR) effect through leaky tumor blood vessels (passive targeting). After going out of the blood vessels, IL-4R-targeting liposomes would bind to IL-4R on tumor cells and enhance their internalization into tumor cells (ligand-mediated or active targeting). These findings indicate that the IL4RPep-1-guided targeting of tumor and tumor blood vessels is a useful strategy for enhancing the delivery of anti-cancer nanocarriers to tumor based on both passive and active targeting.

EPR effect has been considered as a driving force for the extravasation of nanocarriers through tumor blood vessels [21]. However, it was noted that tumors have different pore sizes in the vasculature depending on the types of tumors and have differences in vascular structure even within a single tumor type [22]. In this regard, a ligand that is able to bind to a target protein on tumor endothelial cells may augment tumor vessel-specific accumulation and subsequent extravasation of nanocarriers. To date, only a couple of peptides have been known to target both tumor cells and tumor endothelial cells. These include RGD and NGR peptides, which bind to αvβ3 integrin and

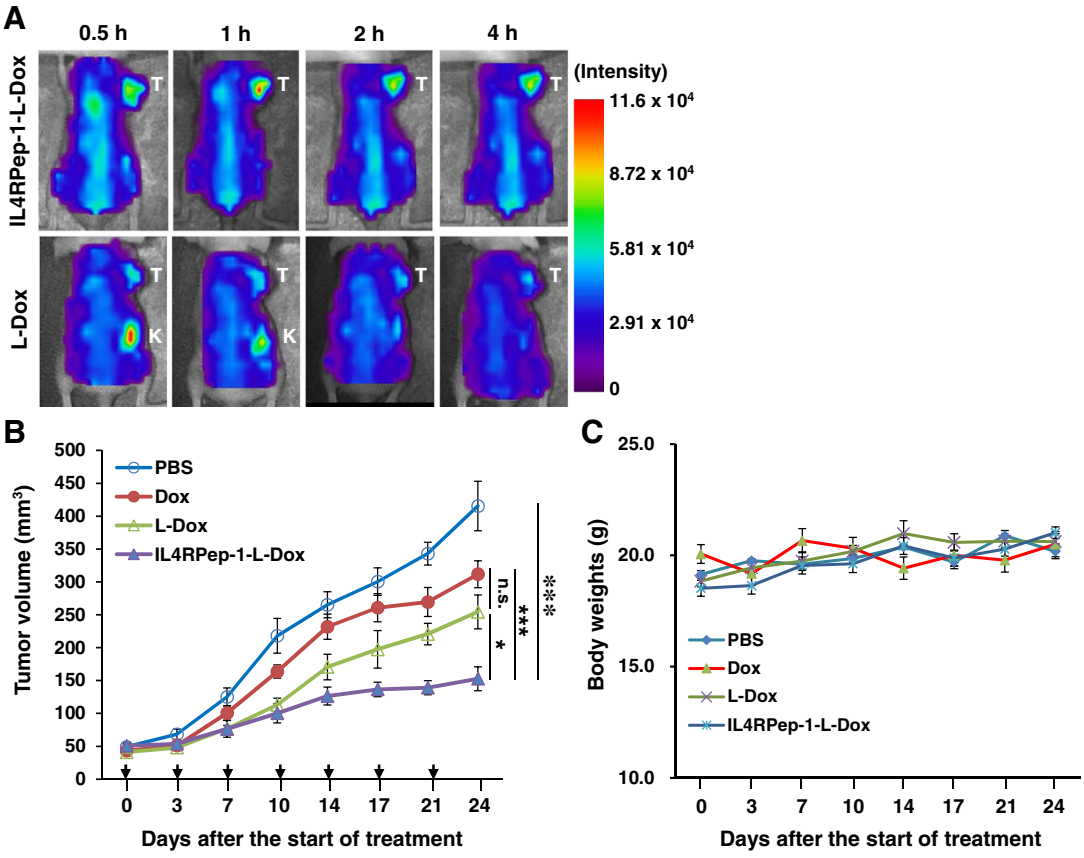

Fig. 5. *In vivo* fluorescence imaging and antitumor growth activity of IL-4R-targeting liposomes. (A) *In vivo* fluorescence imaging. Cy5.5 fluorescence dye-labeled and IL4RPep-1-labeled (IL4RPep-1-L-Dox) or unlabeled (L-Dox) liposomes containing doxorubicin (1 mg/kg) were intravenously injected into H226 tumor-bearing mice. *In vivo* fluorescence images were taken at the indicated time point after injection. A scale bar represents the fluorescence intensity. T, tumor; K, kidney. (B) Antitumor growth activity. Tumor-bearing mice were treated with free doxorubicin (Dox), L-Dox, or IL4RPep-1-L-Dox two times per week for a total of seven injections. Arrows indicate the days of injection. n.s., not significant; *, $p < 0.05$; ***, $p < 0.001$. (C) Body weights of experimental animals during the treatment.

aminopeptidase N, respectively, on both tumor and tumor endothelial cells [23–26]. NGR-coated liposomal doxorubicin, for example, increased apoptosis of tumor cells and tumor endothelial cells, decreased vessel density, and exerted more efficient antitumor activity against neuroblastoma than untargeted liposomal doxorubicin [25,26].

The up-regulation of IL-4R seems to be a common phenotype in the vascular endothelium of cancer and atherosclerosis, where chronic inflammation and cytokine activation of vascular endothelial cells may exist. In the present study, elevation of IL-4R expression was observed on the vascular endothelial cells at tissues of human tumor xenografts on mice, autochthonous transgenic mouse lung cancer, and primary human lung cancer. Increase in IL-4R expression was also observed on HUVECs when activated with TNF-α to mimic an inflammatory microenvironment in tumor blood vessels. The increase of IL-4R on endothelial cells by TNF-α treatment was also reported in a previous study [27]. On the other hand, we have previously reported that IL-4R expression is elevated on the endothelial cells of mouse and human atherosclerotic blood vessels, while little is expressed on the corresponding cells of normal blood vessels [12]. This may explain the reason why IL4RPep-1 was identified by screening of phage-displayed peptide library against atherosclerotic tissues [12].

The IL-4 and IL-4R interaction plays different roles depending on pathologic conditions. In tumors, IL-4 acts as an autocrine growth factor or induces the expression of anti-apoptotic proteins such as Bcl-xL and c-FLIP by tumor cells and contributes to the resistance of cancer cells to chemotherapies [28–32]. In atherosclerosis, IL-4 induces oxidative stress and the expression of vascular cell adhesion molecule-1 and monocyte chemoattractant protein-1 on endothelial cells and contributes to recruitment of monocytes and atherogenesis [33,34].

Mutational analysis showed that the residues C1, R2, R4, L5, R7, and N8 of IL4RPep-1 (^{1}CRKRLDRNC^{9}) were important determinants for its binding. In comparison, the residues R81, K84, R85, R88, N89, and W91 on the homologous sequence of human IL-4 (^{81}RFLKRLDRNLW^{91}) play a role for its binding to IL-4R [35–37]. This suggests that the key binding determinants on IL4RPep-1 are similar with those on the homologous motif that is located in a three-dimensional structure of human IL-4 protein. On mouse IL-4, three arginine residues R80, R83, and R86 (^{79}QRLFRAFR^{86}) are main determinants for its binding to IL-4R [38]. As previously described by us and other group [12,39], three arginine residues on IL4RPep-1 (R2, R4, and R7) and on human IL-4 (R81, R85, and R88) appears to mimic those three arginine residues on mouse IL-4. This may enable IL4RPep-1 to bind to mouse IL-4R as well as human IL-4R. Based on the importance of cysteine at the N-terminal for binding, we saved this cysteine, while deleting cysteine at the C-terminal, for conjugation of IL4RPep-1 to liposomes through thiol group in one direction. Of interest, the binding affinity of IL4RPep-1 to H226 cells (approximately 6.5 μM), determined by the saturation binding assays, was much more higher than that to purified IL-4R on a solid surface (approximately 5.5 mM) that was determined by surface plasmon resonance in a previous study [40]. This suggests the importance of microenvironment in cell membrane for the optimal binding of IL4RPep-1 to IL-4R.

Given the contribution of IL-4 signaling through IL-4R to tumor cell survival and chemoresistance [28–32], IL-4R is not only a target that is up-regulated on tumor but also a potential therapeutic target to be inhibited. In addition, IL-4R expression is correlated with the grade and stage of bladder cancer [41] and the recurrence of oral cavity cancer [42], implicating IL-4R as a prognostic biomarker for cancer management. In these regards, IL-4R would be a promising target for cancer

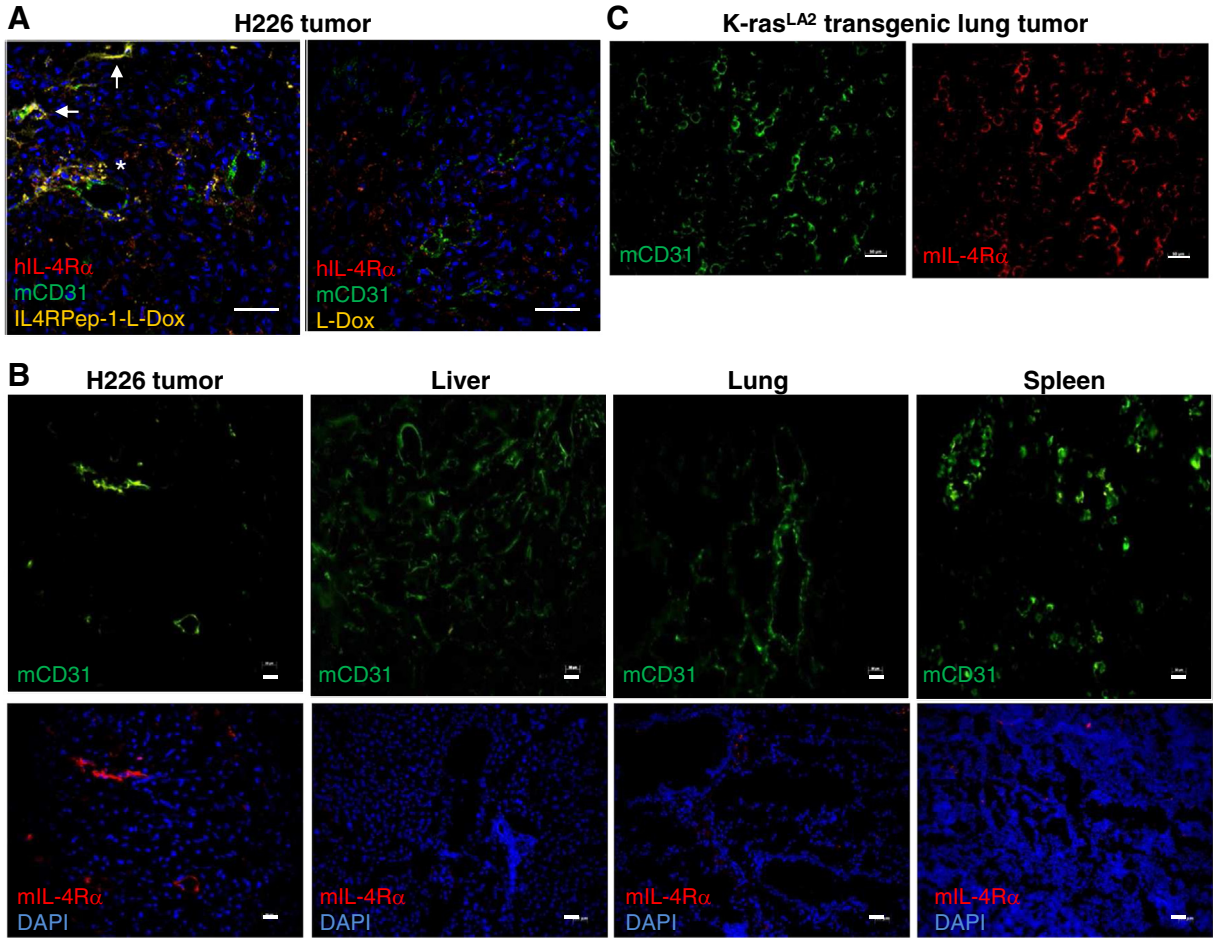

Fig. 6. Accumulation of IL-4R-targeting liposomes and localization of IL-4R at tumor tissues. (A) Accumulation of liposomes at tumor. Cy5.5 fluorescence dye-labeled and IL4RPep-1-labeled (IL4RPep-1-L-Dox) or unlabeled (L-Dox) liposomes were intravenously injected into H226 tumor-bearing mice and circulated for 2 h. Tissue sections were co-stained with anti-human IL-4Rα antibody (hIL-4Rα, red), anti-mouse CD31 antibody (mCD31, green), and DAPI nuclear staining (blue). Note that liposomes (yellow) were accumulated at perivascular tumor cells (asterisk) and blood vessels (arrows). (B) Expression of IL-4R in vascular endothelial cells. Tissue sections of tumor and control organs including liver, lung, and spleen were co-stained with anti-mouse CD31 antibody, anti-mouse IL-4Rα antibody (mIL-4Rα, red), and DAPI nuclear staining. (C) Expression of IL-4R in vascular endothelial cells of K-ras^{LA2} transgenic mouse lung tumor. Tumor tissues were stained with anti-mouse CD31 antibody and anti-mouse IL-4Rα antibody. Scale bars (A-C), 50 μm. (For interpretation of the references to color in this figure legend, the reader is referred to the web version of this article.)

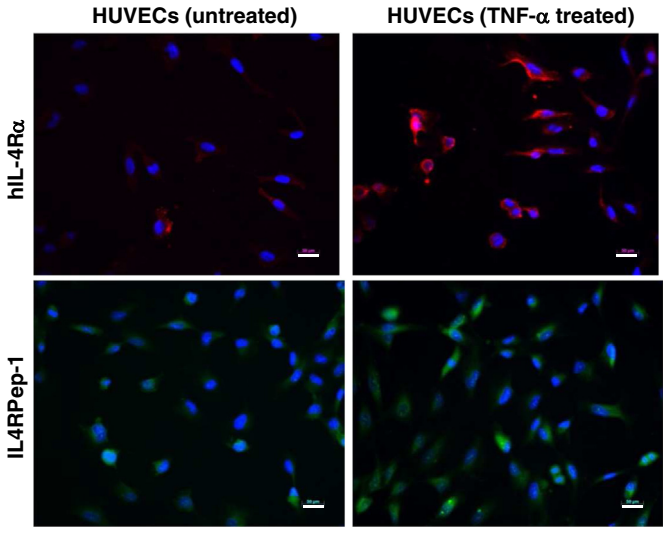

Fig. 7. Up-regulation of IL-4R in TNF-α-activated endothelial cells. HUVECs were activated by TNF-α treatment for 24 h. After treatment, cells were incubated with anti-human IL-4Rα antibody (red) or FITC-labeled IL4RPep-1 (green). Nuclei were counter-stained with DAPI. Scale bars, 50 μM. (For interpretation of the references to color in this figure legend, the reader is referred to the web version of this article.)

therapy. However, it is not ubiquitously expressed at all cases of cancer tissues. In this study, for example, IL-4R was elevated in approximately two thirds of patients with squamous cell carcinoma and adenocarcinoma of NSCLC, while being expressed at low levels in one third of those patients. Similar to our results, the elevated expression of IL-4R has been shown in 66–79% of lung tumor tissues [6]. Overcoming such tumor heterogeneity would need a combination of multiple ligands that recognize different targets or receptors, for example, IL-4R and the mutant EGFR. In the aspects of deep tissue penetration and manufacturing cost, nanocarriers labeled with a combination of multiple peptide

Table 1
IL-4R expression in primary lung cancer tissues.

Specimens	Cases	Weak expression cases (percent)	Strong expression cases (percent)
Squamous cell carcinoma pT1a–pT2b	98	39 (40)	59 (60)
Adenocarcinoma pT1a–pT2b	65	22 (34)	43 (66)
Large cell carcinoma pT1a–pT2a	9	7 (78)	2 (22)

Human primary lung cancer tissues at stages pT1a to pT2b were stained with anti-human IL-4Rα antibody. The IL-4R levels were classified into strong or weak expression according to the staining intensity.

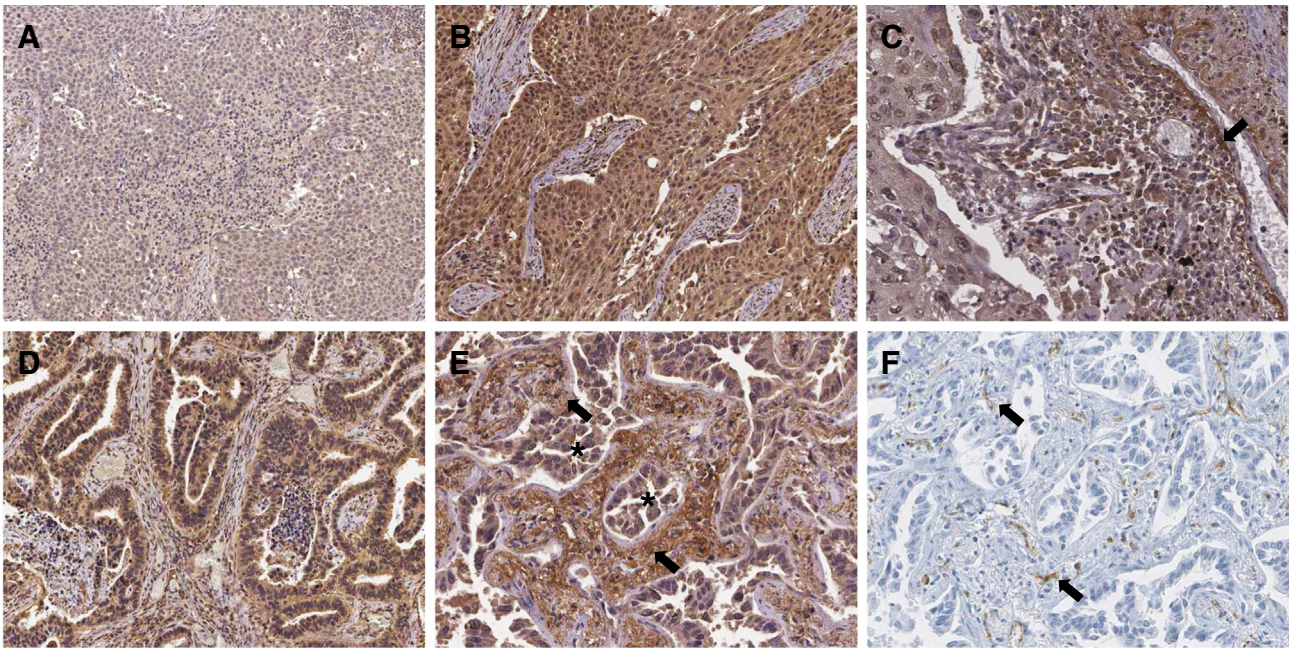

Fig. 8. Expression of IL-4R in primary human lung tumor tissues. Sections of paraffinized tumor tissues were stained with anti-human IL-4Rα antibody and then counterstained with hematoxylin. (A) Staining of squamous cell carcinoma tissue using normal IgG as a negative control. (B) Staining of IL-4R at squamous cell carcinoma tissue. (C) Staining of IL-4R at peritumoral region of squamous cell carcinoma. Note strong staining intensity of IL-4R at peritumoral blood vessels (arrow). (D) Staining of IL-4R at adenocarcinoma tissue. (E) Staining of IL-4R at stroma regions of adenocarcinoma. Note strong staining intensity of IL-4R in tumor-surrounding stroma regions (arrows). Asterisks indicate tumor regions. (F) Staining of blood vessels. Arrows indicate blood vessels in the tumor-surrounding stroma regions at a section parallel to (E).

ligands against multiple targets would be more efficient and practical approach compared to those labeled with antibodies.

Acknowledgments

This work was supported by the grants from the National Research Foundation (NRF) funded by the Korea Government (2012M2A2A7035589 and 2014R1A5A2009242) and the grant from the National R&D Program for Cancer Control, Ministry of Health & Welfare, Korea (0720550–2).

References

[1] C. Zhou, et al., Erlotinib versus chemotherapy as first-line treatment for patients with advanced EGFR mutation-positive non-small-cell lung cancer (OPTIMAL, CTONG-0802): a multicentre, open-label, randomised, phase 3 study, Lancet Oncol. 12 (2011) 735–742.
[2] R. Rosell, et al., Erlotinib versus standard chemotherapy as first-line treatment for European patients with advanced EGFR mutation-positive non-small-cell lung cancer (EURTAC): a multicentre, open-label, randomised phase 3 trial, Lancet Oncol. 13 (2012) 239–246.
[3] C.R. Chong, P.A. Janne, The quest to overcome resistance to EGFR-targeted therapies in cancer, Nat. Med. 19 (2013) 1389–1400.
[4] S. Kobayashi, et al., EGFR mutation and resistance of non-small-cell lung cancer to gefitinib, N. Engl. J. Med. 352 (2005) 786–792.
[5] M. Gerlinger, et al., Intratumor heterogeneity and branched evolution revealed by multiregion sequencing, N. Engl. J. Med. 366 (2012) 883–892.
[6] M. Kawakami, et al., Interleukin 4 receptor on human lung cancer: a molecular target for cytotoxin therapy, Clin. Cancer Res. 8 (2002) 3503–3511.
[7] K. Kawakami, P. Leland, R.K. Puri, Structure, function, and targeting of interleukin 4 receptors on human head and neck cancer cells, Cancer Res. 60 (2000) 2981–2987.
[8] R.K. Puri, Development of a recombinant interleukin-4-*Pseudomonas* exotoxin for therapy of glioblastoma, Toxicol. Pathol. 27 (1999) 53–57.
[9] K. Kawakami, M. Kawakami, R.K. Puri, Overexpressed cell surface interleukin-4 receptor molecules can be successfully targeted for antitumor cytotoxin therapy, Crit. Rev. Immunol. 21 (2001) 299–310.
[10] K. Kawakami, M. Kawakami, S.R. Husain, R.K. Puri, Effect of interleukin (IL)-4 cytotoxin on breast tumor growth after in vivo gene transfer of IL-4 receptor alpha chain, Clin. Cancer Res. 9 (2003) 1826–1836.
[11] T. Shimamura, et al., Interleukin-4 cytotoxin therapy synergizes with gemcitabine in a mouse model of pancreatic ductal adenocarcinoma, Cancer Res. 67 (2007) 9903–9912.
[12] H.Y. Hong, et al., Phage display selection of peptides that home to atherosclerotic plaques: IL-4 receptor as a candidate target in atherosclerosis, J. Cell. Mol. Med. 12 (2008) 2003–2014.
[13] R.C. Ladner, A.K. Sato, J. Gorzelany, M. de Souza, Phage display-derived peptides as therapeutic alternatives to antibodies, Drug Discov. Today 9 (2004) 525–529.
[14] S. Lee, J. Xie, X. Chen, Peptides and peptide hormones for molecular imaging and disease diagnosis, Chem. Rev. 110 (2010) 3087–3111.
[15] E. Ruoslahti, Peptides as targeting elements and tissue penetration devices for nanoparticles, Adv. Mater. 24 (2012) 3747–3756.
[16] R. Namgung, et al., Poly-cyclodextrin and poly-paclitaxel nano-assembly for anticancer therapy, Nat. Commun. 5 (2014) 3702.
[17] X.L. Wu, et al., Tumor-targeting peptide conjugated pH-responsive micelles as a potential drug carrier for cancer therapy, Bioconjug. Chem. 21 (2010) 208–213.
[18] F.Y. Yang, et al., Focused ultrasound and interleukin-4 receptor-targeted liposomal doxorubicin for enhanced targeted drug delivery and antitumor effect in glioblastoma multiforme, J. Control. Release 160 (2012) 652–658.
[19] J.H. Kim, et al., Facilitated intracellular delivery of peptide-guided nanoparticles in tumor tissues, J. Control. Release 157 (2012) 493–499.
[20] L. Johnson, et al., Somatic activation of the K-ras oncogene causes early onset lung cancer in mice, Nature 410 (2001) 1111–1116.
[21] Y. Matsumura, H. Maeda, A new concept for macromolecular therapeutics in cancer chemotherapy: mechanism of tumoritropic accumulation of proteins and the antitumor agent smancs, Cancer Res. 46 (1986) 6387–6392.
[22] U. Prabhakar, et al., Challenges and key considerations of the enhanced permeability and retention effect for nanomedicine drug delivery in oncology, Cancer Res. 73 (2013) 2412–2417.
[23] R.M. Schiffelers, et al., Anti-tumor efficacy of tumor vasculature-targeted liposomal doxorubicin, J. Control. Release 91 (2003) 115–122.
[24] S. Zitzmann, V. Ehemann, M. Schwab, Arginine-glycine-aspartic acid (RGD)-peptide binds to both tumor and tumor-endothelial cells in vivo, Cancer Res. 62 (2002) 5139–5143.
[25] F. Pastorino, et al., Targeting liposomal chemotherapy via both tumor cell-specific and tumor vasculature-specific ligands potentiates therapeutic efficacy, Cancer Res. 66 (2006) 10073–10082.
[26] F. Pastorino, et al., Vascular damage and anti-angiogenic effects of tumor vessel-targeted liposomal chemotherapy, Cancer Res. 63 (2003) 7400–7409.
[27] S.M. Lugli, et al., Tumor necrosis factor alpha enhances the expression of the interleukin (IL)-4 receptor alpha-chain on endothelial cells increasing IL-4 or IL-13-induced Stat6 activation, J. Biol. Chem. 272 (1997) 5487–5494.
[28] C. Conticello, et al., IL-4 protects tumor cells from anti-CD95 and chemotherapeutic agents via up-regulation of antiapoptotic proteins, J. Immunol. 172 (2004) 5467–5477.
[29] O. Prokopchuk, Y. Liu, D. Henne-Bruns, M. Kornmann, Interleukin-4 enhances proliferation of human pancreatic cancer cells: evidence for autocrine and paracrine actions, Br. J. Cancer 92 (2005) 921–928.
[30] M. Todaro, et al., Colon cancer stem cells dictate tumor growth and resist cell death by production of interleukin-4, Cell Stem Cell 1 (2007) 389–402.

[31] M. Todaro, et al., Apoptosis resistance in epithelial tumors is mediated by tumor-cell-derived interleukin-4, Cell Death Differ. 15 (2008) 762–772.
[32] M. Todaro, et al., Autocrine production of interleukin-4 and interleukin-10 is required for survival and growth of thyroid cancer cells, Cancer Res. 66 (2006) 1491–1499.
[33] Y.W. Lee, et al., IL-4-induced oxidative stress upregulates VCAM-1 gene expression in human endothelial cells, J. Mol. Cell. Cardiol. 33 (2001) 83–94.
[34] L. Walch, et al., Pro-atherogenic effect of interleukin-4 in endothelial cells: modulation of oxidative stress, nitric oxide and monocyte chemoattractant protein-1 expression, Atherosclerosis 187 (2006) 285–291.
[35] Y. Wang, B.J. Shen, W. Sebald, A mixed-charge pair in human interleukin 4 dominates high-affinity interaction with the receptor alpha chain, Proc. Natl. Acad. Sci. U. S. A. 94 (1997) 1657–1662.
[36] T. Hage, W. Sebald, P. Reinemer, Crystal structure of the interleukin-4/receptor alpha chain complex reveals a mosaic binding interface, Cell 97 (1999) 271–281.
[37] T.D. Mueller, J.L. Zhang, W. Sebald, A. Duschl, Structure, binding, and antagonists in the IL-4/IL-13 receptor system, Biochim. Biophys. Acta 1592 (2002) 237–250.
[38] G. Yao, et al., Identification of core functional region of murine IL-4 using peptide phage display and molecular modeling, Int. Immunol. 18 (2006) 19–29.
[39] L. Yang, et al., Targeting interleukin-4 receptor alpha with hybrid peptide for effective cancer therapy, Mol. Cancer Ther. 11 (2012) 235–243.
[40] V. Sarangthem, et al., Construction and application of elastin like polypeptide containing IL-4 receptor targeting peptide, PLoS One 8 (2013) e81891.
[41] B.H. Joshi, et al., Interleukin-4 receptor alpha overexpression in human bladder cancer correlates with the pathological grade and stage of the disease, Cancer Med. 3 (2014) 1615–1628.
[42] M. Kwon, et al., Recurrence and cancer-specific survival according to the expression of IL-4Ralpha and IL-13Ralpha1 in patients with oral cavity cancer, Eur. J. Cancer 51 (2015) 177–185.